Connection Between Damping Torque Analysis and Energy Flow Analysis in Damping Performance Evaluation for Electromechanical Oscillations in Power Systems

Yong Hu, Siqi Bu, Xin Zhang, Chi Yung Chung, and Hui Cai

***Abstract*—The damping performance evaluation for electromechanical oscillations in power systems is crucial for the stable operation of modern power systems. In this paper, the connection between two commonly-used damping performance evaluation methods, i.e., the damping torque analysis (DTA) and energy flow analysis (EFA), are systematically examined and revealed for the better understanding of the oscillatory damping mechanism. First, a concept of the aggregated damping torque coefficient is proposed and derived based on DTA of multi-machine power systems, which can characterize the integration effect of the damping contribution from the whole power system. Then, the pre-processing of measurements at the terminal of a local generator is conducted for EFA, and a concept of the frequency-decomposed energy attenuation coefficient is defined to screen the damping contribution with respect to the interested frequency. On this basis, the frequency spectrum analysis of the energy attenuation coefficient is employed to rigorously prove that the results of DTA and EFA are essentially equivalent, which is valid for arbitrary types of synchronous generator models in multi-machine power systems. Additionally, the consistency between the aggregated damping torque coefficient and frequency-decomposed energy attenuation coefficient is further verified by the numerical calculation in case studies. The relationship between the proposed coefficients and the eigenvalue (or damping ratio) is finally revealed, which consolidates the application of the proposed concepts in the damping performance evaluation.**

***Index Terms*—Electromechanical oscillation, damping performance, damping torque analysis (DTA), energy flow analysis (EFA), frequency spectrum.**

I. Introduction

ELECTROMECHANICAL oscillation is an inherent phenomenon in modern power systems, which is of many concerns in the large-scale or interconnected system operation [1]. The oscillation events can be triggered by various factors such as the sudden change in transmission line parameters, generator faults, and load fluctuations [2], [3]. Over the past several years, a series of oscillation incidents have occurred in power systems all over the world, e.g., several events observed in USA [4], [5] and China [6]. These oscillation incidents have posed critical threats to the stable operation of power systems.

After an oscillation accident occurs, if the oscillatory power lasts for a while and then gradually decays, the oscillation is considered to be stable. The damping is a quantitative characterization to evaluate the oscillatory stability, and the better damping performance indicates a shorter oscillation duration. For the power systems with weak natural damping, the damping performance is normally enhanced by using the external equipment such as the power system stabilizers (PSSs) [7], [8]. The damping performance evaluation should be carefully conducted for the installation planning and parameter setting of PSSs. At present, there are two commonly-used methods for the damping performance evaluation, i.e., the damping torque analysis (DTA) and energy flow analysis (EFA).

DTA originates from the concept of the electric torque of synchronous generators in the electromechanical oscillation. The generator rotor movement produces the torque effect, which provides a clear physical explanation [9], [10]. As a component of the electric torque, the damping torque contributes to the damping of power oscillations [9]. At present, DTA is a common method to examine the effect of excitation control on the small-signal stability of power systems and is gradually extended to the damping performance evaluation as well as the design of stabilizer controllers. DTA is a mathematical modeling-based method. The mathematical

Manuscript received: June 28, 2020; revised: October 19, 2020; accepted: December 3, 2020. Date of CrossCheck: December 3, 2020. Date of online publication: February 17, 2021.

This work was supported in part by the National Natural Science Foundation of China (No. 51807171), the Guangdong Science and Technology Department (No. 2019A1515011226), the Hong Kong Research Grant Council (No. 15200418), and the Department of Electrical Engineering, The Hong Kong Polytechnic University for the Start-up Fund (No. 1-ZE68).

Y. Hu and S. Bu (corresponding author) are with the Department of Electrical Engineering and Research Institute for Smart Energy, The Hong Kong Polytechnic University, Hong Kong, China, and they are also with the Shenzhen Research Institute, The Hong Kong Polytechnic University, Shenzhen, China (e-mail: yong68.hu@connect.polyu.hk; siqi.bu@polyu.edu.hk).

X. Zhang is with the Centre for Energy Systems and Strategy, Cranfield University, Cranfield, UK (e-mail: xin.zhang@cranfield.ac.uk).

C. Y. Chung is with the Department of Electrical and Computer Engineering, University of Saskatchewan, Saskatoon, Canada (e-mail: c.y.chung@usask.ca).

H. Cai is with the State Grid Jiangsu Economic Research Institute, Nanjing, China (e-mail: caihui300@hotmail.com).

DOI: 10.35833/MPCE.2020.000413

models of the doubly-fed induction generator (DFIG), fixed-speed induction generator, and three transitional wound rotor generators are established in [11] to realize the damping torque assessment. A model reduction strategy of DFIGs is mathematically proposed in [12] to improve the efficiency of the dynamic DTA. The dynamic mathematical model of DFIGs with the least order but acceptable accuracy is established in [13] to investigate the damping torque from different dynamic components of DFIGs. DTA is proven to be equivalent to the conventional eigenvalue-based analysis [14].

The damping torque coefficient is an important index to represent the relationship between the damping torque and angular frequency. References [15]-[17] study the damping torque coefficient through the state-space modeling based on a linearized model. In a single-machine infinite-bus power system, there is only one dominant oscillation mode and the damping torque coefficient can directly characterize the damping performance of the whole power system. However, the damping torque coefficients of multiple generators are presented in the matrix form for multi-machine power systems [9]. The damping contribution of the whole power system is distributed to the generators associated with the oscillation mode, which makes the analysis more complex for multi-machine power systems. There is a lack of a useful concept for DTA that can characterize the integration effect of the damping contribution from the whole power system, which should be applicable for arbitrary types of synchronous generator models in multi-machine power systems.

The electromechanical oscillation events are accompanied by the transmission and dissipation of the oscillatory energy flow in the power system. For a stable oscillation event, the oscillatory energy flow is eventually dissipated by the generators as well as external stabilizers. Hence, the EFA provides a clear description for the electromechanical oscillation mechanism. In recent years, the phasor measurement unit (PMU) and wide area measurement system (WAMS) have been applied in the power system stability analysis [18], [19], which facilitates the measurement of the oscillatory energy flow at the terminal of a local generator. The measurement-based EFA becomes an emerging way to evaluate the damping performance. Compared with DTA, EFA shows an apparent advantage: no complex modeling process is required, especially for the large-scale power system.

The basic components of the oscillatory energy flow are presented in [20] and the oscillatory energy flow is utilized to determine the location of oscillation sources. In [21], the numerical estimation of the damping performance is provided by analyzing the rate of change of the oscillatory energy flow. In [22], the oscillatory energy flow is linked with the electric torque from the perspective of physics and attempt to expand the damping torque coefficient to a frequency spectrum. However, the connection between EFA and DTA is not mathematically explored in [21] and [22]. The consistency of EFA and DTA tends to be revealed in [23]-[25], but all the derivations are unfortunately restricted to a certain simplified model of synchronous generators, which largely reduces the generality and significance of the work. Therefore, there is no research so far to rigorously justify the consistency between EFA and DTA for the damping performance evaluation. In addition, the measurement at the terminal of a local generator involves multiple oscillation modes with respect to different frequencies in the multi-machine power system; thus, the pre-processing of the measurements at the terminal of a local generator should be conducted so that the damping contribution with respect to the interested frequency can be screened.

Considering all the points above, the major contributions of this paper are listed as follows.

1) For DTA, in order to characterize the integration effect of the damping contribution from the whole power system, a concept of the aggregated damping torque coefficient is proposed and derived. It can be applied to arbitrary types of synchronous generator models in multi-machine power systems. The aggregated damping torque coefficient lays a foundation for identifying the theoretical connection between DTA and EFA.

2) For EFA, the pre-processing of measurements at the terminal of a local generator is conducted in the time domain. Based on that, a concept of the frequency-decomposed energy attenuation coefficient is defined to pick out the damping contribution with respect to the interested frequency.

3) The connection between DTA and EFA is strictly proven and the consistency of the aggregated damping torque coefficient and frequency-decomposed energy attenuation coefficient is revealed, which is a general conclusion for arbitrary types of synchronous generator models in both single-machine infinite-bus power systems and multi-machine power systems.

4) The relationship between the frequency-decomposed energy attenuation coefficient (or aggregated damping torque coefficient) and the corresponding eigenvalue as well as damping ratio is revealed based on the numerical calculation and hence the application of the former proposed concepts in the damping performance evaluation can be further verified and consolidated.

The rest of this paper is organized as follows. Section II presents a DTA in the frequency domain and defines the aggregated damping torque coefficient. In Section III, EFA is conducted based on the pre-processing of measurements in the time domain and the frequency-decomposed energy attenuation coefficient is defined. The frequency spectrum analysis of the energy attenuation coefficient is conducted in Section IV, which reveals the connection between DTA and EFA. Case studies are carried out in Section V. Finally, conclusions are drawn in Section VI.

II. DTA in Frequency Domain

In this section, a DTA is conducted in the frequency domain via the mathematical modeling. Compared with the Phillips-Heffron model-based analysis in [9], the derivations presented in this section are order-independent for the synchronous generator models and can effectively evaluate the integration effect of the damping contribution from multi-machine power systems.

The swing equation of the i^{th} generator in a power system

is expressed as:

$$\begin{cases} \dfrac{\mathrm{d}\delta_i}{\mathrm{d}t} = \omega_0(\omega_i - 1) \\ \dfrac{\mathrm{d}\omega_i}{\mathrm{d}t} = \dfrac{1}{T_{Ji}}[P_{mi} - P_{ei} - D_i(\omega_i - 1)] \end{cases} \tag{1}$$

where δ_i is the power angle of the i^{th} generator; ω_0 is the synchronous angular frequency; ω_i is the angular frequency of the i^{th} generator; T_{Ji} is the inertia constant of the i^{th} generator; P_{mi} is the mechanical power of the i^{th} generator; P_{ei} is the electric power of the i^{th} generator; and D_i is the natural damping of the i^{th} generator. It should be noted that i is omitted for a single-machine infinite-bus power system.

For DTA, some other equations should be further involved besides (1), e. g., the equations that characterize automatic voltage regulators (AVRs), PSSs, etc. Define a vector $\boldsymbol{Z}$ that includes the state variables of the generator(s) except δ_i and ω_i. The dimension of $\boldsymbol{Z}$ is $\left(\sum_{i=1}^{k} n_i - 2\right) \times 1$, where n_i is the order of the i^{th} generator model and k is the number of the generator(s). Then, the linearized model of a power system can be derived as:

$$\begin{bmatrix} \dfrac{\mathrm{d}\Delta\delta_i(t)}{\mathrm{d}t} \\ \dfrac{\mathrm{d}\Delta\omega_i(t)}{\mathrm{d}t} \\ \dfrac{\mathrm{d}\Delta\boldsymbol{Z}(t)}{\mathrm{d}t} \end{bmatrix} = \begin{bmatrix} 0 & \omega_0 & \boldsymbol{0} \\ A_{21} & -\dfrac{D_i}{T_{Ji}} & \boldsymbol{A}_{23} \\ \boldsymbol{A}_{31} & \boldsymbol{A}_{32} & \boldsymbol{A}_{33} \end{bmatrix} \begin{bmatrix} \Delta\delta_i(t) \\ \Delta\omega_i(t) \\ \Delta\boldsymbol{Z}(t) \end{bmatrix} \tag{2}$$

where A_{21} is the element of the state matrix; $\boldsymbol{A}_{23}$, $\boldsymbol{A}_{31}$, $\boldsymbol{A}_{32}$, and $\boldsymbol{A}_{33}$ are the block sub-matrices of the state matrix; $\Delta\delta_i(t)$ is the power angle deviation of the i^{th} generator in the time domain; $\Delta\omega_i(t)$ is the angular frequency deviation of the i^{th} generator in the time domain; and $\Delta\boldsymbol{Z}(t)$ is the deviation of the state variables aggregated in $\boldsymbol{Z}$ in the time domain.

The representation of (2) is transformed from time domain to frequency domain applying the Fourier transform, as given by:

$$\begin{bmatrix} \Delta\delta_i(f) \\ \Delta\omega_i(f) \\ \Delta\boldsymbol{Z}(f) \end{bmatrix} = \frac{1}{\mathrm{j}2\pi f} \begin{bmatrix} 0 & \omega_0 & 0 \\ A_{21} & -\dfrac{D_i}{T_{Ji}} & \boldsymbol{A}_{23} \\ \boldsymbol{A}_{31} & \boldsymbol{A}_{32} & \boldsymbol{A}_{33} \end{bmatrix} \begin{bmatrix} \Delta\delta_i(f) \\ \Delta\omega_i(f) \\ \Delta\boldsymbol{Z}(f) \end{bmatrix} \tag{3}$$

where $\Delta\delta_i(f)$ is the power angle deviation of the i^{th} generator in the frequency domain; $\Delta\omega_i(f)$ is the angular frequency deviation of the i^{th} generator in the frequency domain; and $\Delta\boldsymbol{Z}(f)$ is the deviation of the state variables aggregated in $\boldsymbol{Z}$ in the frequency domain.

Based on (1) and (3), the linearized representation of a power system can be derived as the form in Fig. 1.

From Fig. 1, the relationships among the major variables are clearly revealed. Then, (4)-(6) can be derived, respectively.

$$\Delta P_{ei}(f) = -T_{Ji}(A_{21}\Delta\delta_i(f) + \boldsymbol{A}_{23}\Delta\boldsymbol{Z}(f)) \tag{4}$$

$$\Delta\delta_i(f) = \frac{\omega_0}{\mathrm{j}2\pi f}\Delta\omega_i(f) \tag{5}$$

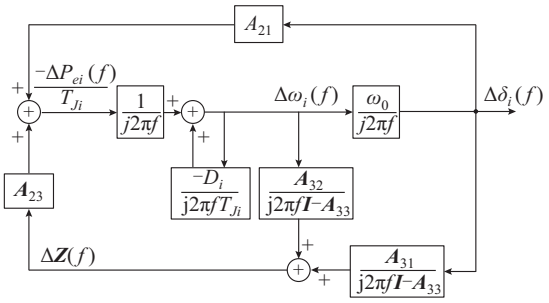

Fig. 1. Linearized representation of a power system.

$$\Delta\boldsymbol{Z}(f) = \frac{\boldsymbol{A}_{31}}{\mathrm{j}2\pi f\boldsymbol{I} - \boldsymbol{A}_{33}}\Delta\delta_i(f) + \frac{\boldsymbol{A}_{32}}{\mathrm{j}2\pi f\boldsymbol{I} - \boldsymbol{A}_{33}}\Delta\omega_i(f) \tag{6}$$

where $\Delta P_{ei}(f)$ is the electric power deviation of the i^{th} generator in the frequency domain; and $\boldsymbol{I}$ is an identity matrix.

Substitute (5) and (6) into (4), and (7) can be derived step by step.

$$\begin{aligned} &\Delta P_{ei}(f) = -T_{Ji}(A_{21}\Delta\delta_i(f) + \boldsymbol{A}_{23}\Delta\boldsymbol{Z}(f)) = \\ &-T_{Ji}\left[\left(A_{21} + \boldsymbol{A}_{23}\frac{\boldsymbol{A}_{31}}{\mathrm{j}2\pi f\boldsymbol{I} - \boldsymbol{A}_{33}}\right)\Delta\delta_i(f) + \boldsymbol{A}_{23}\frac{\boldsymbol{A}_{32}}{\mathrm{j}2\pi f\boldsymbol{I} - \boldsymbol{A}_{33}}\Delta\omega_i(f)\right] = \\ &-T_{Ji}\left[\left(A_{21} + \boldsymbol{A}_{23}\frac{\boldsymbol{A}_{31}}{\mathrm{j}2\pi f\boldsymbol{I} - \boldsymbol{A}_{33}}\right)\frac{\omega_0}{\mathrm{j}2\pi f} + \boldsymbol{A}_{23}\frac{\boldsymbol{A}_{32}}{\mathrm{j}2\pi f\boldsymbol{I} - \boldsymbol{A}_{33}}\right]\Delta\omega_i(f) \end{aligned} \tag{7}$$

The electric torque consists of two components: the damping torque and synchronous torque. According to the discussion in the introduction, the damping torque contributes to the damping of power oscillations. Since the rotating speed is close to 1 p.u., the electric power is approximately equal to the electric torque. According to the definition of the damping torque, the real part of the ratio of $\Delta P_{ei}(f)$ and $\Delta\omega_i(f)$, i.e., $K_{da,i}(f)$ in (8) can be regarded as the damping torque coefficient. Equations (7) and (8) will play an important role in revealing the connection between DTA and EFA in Section IV.

$$\begin{aligned} &K_{da,i}(f) = \\ &\mathrm{Re}\left\{-T_{Ji}\left[\left(A_{21} + \boldsymbol{A}_{23}\frac{\boldsymbol{A}_{31}}{\mathrm{j}2\pi f\boldsymbol{I} - \boldsymbol{A}_{33}}\right)\frac{\omega_0}{\mathrm{j}2\pi f} + \boldsymbol{A}_{23}\frac{\boldsymbol{A}_{32}}{\mathrm{j}2\pi f\boldsymbol{I} - \boldsymbol{A}_{33}}\right]\right\} \end{aligned} \tag{8}$$

where $\mathrm{Re}\{\cdot\}$ is the real part operator.

For a single-machine infinite-bus power system, (8) is actually the damping torque coefficient of this single generator according to the traditional definition of the damping torque.

For a multi-machine power system, as explained in Section I, the damping torque coefficients of multiple generators are usually presented in the matrix form. Equation (8) essentially implies the integration effect of the damping contribution from the whole power system but projected to the i^{th} generator, which is different from the traditional definition of the damping torque. Hence, a useful concept is given as Definition 1.

Definition 1: the aggregated damping torque coefficient of the i^{th} generator with respect to the interested oscillation frequency f_d is defined as $K_{da,i}(f_d)$ by substituting f_d into (8).

The physical explanation of this concept is that all the

damping contributions from the whole power system are aggregated and then reflected from a selected generator.

III. EFA in Time Domain

As indicated in [23] and [24], the oscillatory energy flow from node a to node b can be calculated by:

$$\begin{aligned} W_{ab} &= \int [P_{ab}\mathrm{d}\theta_a + Q_{ab}\mathrm{d}(\ln U_a)] = \int (P_{ab,s} + \Delta P_{ab})\,\mathrm{d}(\theta_{a,s} + \Delta\theta_a) + \\ &\int (Q_{ab,s} + \Delta Q_{ab})\,\mathrm{d}(\ln(U_{a,s} + \Delta U_a)) = \int P_{ab,s}\mathrm{d}\Delta\theta_a + \\ &\int \Delta P_{ab}\mathrm{d}\Delta\theta_a + (Q_{ab,s} + \Delta Q_{ab})\mathrm{d}(\ln(U_{a,s} + \Delta U_a)) \end{aligned} \tag{9}$$

where W_{ab} is the oscillatory energy flow from node a to node b; P_{ab} is the active power flow from node a to node b; Q_{ab} is the reactive power flow from node a to node b; U_a and θ_a are the amplitude and phase angle of the voltage of node a; the subscript s denotes the steady-state value of corresponding variable; and the operator $\Delta(\cdot)$ denotes the deviation of corresponding variable from its steady-state value.

Normally, the reactive power in (9) is ignored. Then, it can be observed that the oscillatory energy flow in (9) consists of two components, as listed in (10).

$$\begin{cases} W_{ab}^1 = \int P_{ab,s}\mathrm{d}\Delta\theta_a \\ W_{ab}^2 = \int \Delta P_{ab}\mathrm{d}\Delta\theta_a \end{cases} \tag{10}$$

where W_{ab}^1 is the oscillatory energy component with respect to $P_{ab,s}$; and W_{ab}^2 is the oscillatory energy component with respect to ΔP_{ab}, which reflects the dissipation of the oscillatory energy flow [23].

The electric power of the generator is considered to be numerically equal to the active power flow between the two nodes, and the phase angle of the node voltage is approximately regarded as the power angle of the generator. On this basis, the oscillatory energy flow dissipated by the i^{th} generator can be calculated by (11) using the measurements at the terminal of a local generator.

$$W_i = \Delta P_{ei}(t)\mathrm{d}\Delta\delta_i(t) \tag{11}$$

where W_i is the oscillatory energy flow dissipated by the i^{th} generator; and $\Delta P_{ei}(t)$ is the electric power deviation of the i^{th} generator in the time domain.

Since the rotating speed is close to 1 p.u., the electric power is approximately equal to the electric torque. Then, the oscillatory energy flow dissipated by the i^{th} generator can also be represented as:

$$W_i = \omega_0 \int \Delta T_{ei}(t)\Delta\omega_i(t)\mathrm{d}t \tag{12}$$

where $\Delta T_{ei}(t)$ is the electric torque deviation of the i^{th} generator.

Generally, the electric torque can be divided into synchronizing torque and damping torque [9], which can be expressed as:

$$\Delta T_{ei}(t) = K_{di}\Delta\omega_i(t) + K_{si}\Delta\delta_i(t) \tag{13}$$

where K_{di} is the damping torque coefficient of the i^{th} generator; and K_{si} is the synchronizing torque coefficient of the i^{th} generator.

The integral of the product of power angle deviation and angular frequency deviation is equal to zero, and then (14) can be further derived based on (11)-(13).

$$\int \Delta P_{ei}(t)\mathrm{d}\Delta\delta_i(t) = \omega_0 \int K_{di}\Delta\omega_i^2(t)\mathrm{d}t \tag{14}$$

The damping torque coefficient can be derived from (14), as given by:

$$K_{di} = \frac{\int_0^{+\infty} \Delta P_{ei}(t)\mathrm{d}\Delta\delta_i(t)}{\omega_0 \int_0^{+\infty} \Delta\omega_i^2(t)\mathrm{d}t} \tag{15}$$

K_{di} can reflect the energy attenuation brought by the damping torque of generators, and hence we define the calculation result of (15) as the energy attenuation coefficient. Using the measurements at the terminal of a local generator, the energy attenuation coefficient of the i^{th} generator can be estimated by:

$$K_{de,i} = \frac{\int_0^{+\infty} \Delta P_{ei}(t)\Delta\omega_i(t)\mathrm{d}t}{\int_0^{+\infty} \Delta\omega_i^2(t)\mathrm{d}t} \tag{16}$$

where $K_{de,i}$ is the energy attenuation coefficient of the i^{th} generator based on EFA.

For a single-machine infinite-bus power system, the measurement at the terminal of a generator involves only one oscillation mode. Equation (16) can be directly used to estimate the energy attenuation coefficient of this single generator.

For a multi-machine power system, the measurement at the terminal of a local generator involves multiple oscillation modes. It is difficult to directly estimate the energy attenuation coefficient using (16). Therefore, it is necessary to conduct the pre-processing for the measurements at the terminal of a local generator in the time domain. According to the theory of Fourier series, any signal that satisfies the Dirichlet condition can be decomposed into a series of sub-signals, as given by:

$$g(t) = \sum_{j=0}^{\infty} A_j \cos(2\pi f_j t + \alpha_j) \tag{17}$$

where $g(t)$ is a signal in the time domain; A_j is the amplitude of the j^{th} sub-signal; f_j is the frequency of the j^{th} sub-signal; and α_j is the phase angle of the j^{th} sub-signal.

The amplitude-frequency characteristic and phase-frequency characteristic of $g(t)$ can be obtained by the well-known Fourier transform, as shown in (18)-(20).

$$G(f) = F(g(t)) = \int_{-\infty}^{+\infty} g(t)\mathrm{e}^{-\mathrm{j}2\pi ft}\,\mathrm{d}t \tag{18}$$

$$\boldsymbol{A}_{1\times p} = \left| [G(f_0) \quad G(f_1) \quad \cdots \quad G(f_{p-1})] \right| \tag{19}$$

$$\boldsymbol{\alpha}_{1\times p} = \arg([G(f_0) \quad G(f_1) \quad \cdots \quad G(f_{p-1})]) \tag{20}$$

where $G(f)$ is the Fourier transform of $g(t)$; $\boldsymbol{A}_{1\times p}$ is the p-dimension vector that includes the amplitudes of sub-signals at each frequency; $\boldsymbol{\alpha}_{1\times p}$ is the p-dimension vector that includes the phase angles of sub-signals at each frequency; $|\cdot|$ denotes the magnitude of a complex number; and $\arg(\cdot)$ denotes the phase angle of a complex number.

The amplitude $A_d \in \boldsymbol{A}_{1\times p}$ and phase angle $\alpha_d \in \boldsymbol{\alpha}_{1\times p}$ at the interested oscillation frequency f_d can be observed from the

amplitude-frequency characteristic and phase-frequency characteristic of $g(t)$, and then the decomposed sub-signal with respect to the interested oscillation frequency f_d is given as:

$$g^{f_d}(t)=A_d\cos(2\pi f_d t+\alpha_d) \tag{21}$$

where $g^{f_d}(t)$ is the decomposed sub-signal from $g(t)$ with respect to f_d.

Based on (18) - (21), the decomposition is conducted for the electric power deviation and angular frequency deviation of the i^{th} generator, and the decomposed sub-signals with respect to f_d are substituted into (16) to screen the damping contribution with respect to f_d, as shown in (22). A concept is given as Definition 2.

Definition 2: the frequency-decomposed energy attenuation coefficient of the i^{th} generator with respect to an interested oscillation frequency f_d is defined as $K_{de,i}^{f_d}$ by (22).

$$K_{de,i}^{f_d}=\frac{\int_0^{+\infty}\Delta P_{ei}^{f_d}(t)\Delta\omega_i^{f_d}(t)\mathrm{d}t}{\int_0^{+\infty}(\Delta\omega_i^{f_d}(t))^2\mathrm{d}t} \tag{22}$$

where $\Delta P_{ei}^{f_d}(t)$ is the decomposed sub-signal from $\Delta P_{ei}(t)$ with respect to f_d; and $\Delta\omega_i^{f_d}(t)$ is the decomposed sub-signal from $\Delta\omega_i(t)$ with respect to f_d.

If we repeat the calculation in (22) with respect to multiple oscillation frequencies, e. g., f_a, f_b, f_c, …, the set $\left\{K_{de,i}^{f_a},K_{de,i}^{f_b},K_{de,i}^{f_c},\ldots\right\}$ can be obtained. It can be observed that the frequency-decomposed energy attenuation coefficients calculated in the time domain can be represented as a spectrum with respect to multiple oscillation frequencies, which will be further analyzed in the Section IV.

In the case studies, i. e., Section V, the time-domain data of the electric power and angular frequency can be obtained by the real-life measurements or solving differential equations. In this paper, the time-domain data of the electric power and angular frequency are obtained by solving the differential equations based on synchronous generator models. The power flow calculation is needed in the process of solving differential equations.

IV. Consistency Between EFA and DTA

In this section, the frequency spectrum analysis of the energy attenuation coefficient is conducted to demonstrate the consistency between EFA and DTA.

Using Parseval's theorem, the integral of the product of two real signals in the time domain can be conducted equivalently in the frequency domain, i. e., (23). It is noted that $g_1(t)=0$ and $g_2(t)=0$ when $t<0$.

$$\int_{-\infty}^{+\infty}g_1(t)g_2(t)\mathrm{d}t=\int_{-\infty}^{+\infty}G_1(f)G_2^*(f)\mathrm{d}f=\int_{-\infty}^{+\infty}G_1^*(f)G_2(f)\mathrm{d}f \tag{23}$$

where $g_1(t)$ and $g_2(t)$ are two signals in the time domain; $G_1(f)$ and $G_2(f)$ are the Fourier transforms of $g_1(t)$ and $g_2(t)$, respectively; and $*$ is the conjugate operator.

Let $G_1(f)=R_1(f)+\mathrm{j}X_1(f)$ and $G_2(f)=R_2(f)+\mathrm{j}X_2(f)$, and then (24) can be derived.

$$\begin{aligned}G_1(f)G_2^*(f)&=(R_1(f)+\mathrm{j}X_1(f))(R_2(f)-\mathrm{j}X_2(f))=\\&X_1(f)X_2(f)+\mathrm{j}(R_2(f)X_1(f)-R_1(f)X_2(f))\end{aligned} \tag{24}$$

According to the definition of Fourier transform, (25) can be derived.

$$\begin{cases}R_1(f)=\int_{-\infty}^{+\infty}g_1(t)\cos(2\pi ft)\mathrm{d}t\\X_1(f)=-\int_{-\infty}^{+\infty}g_1(t)\sin(2\pi ft)\mathrm{d}t\\R_2(f)=\int_{-\infty}^{+\infty}g_2(t)\cos(2\pi ft)\mathrm{d}t\\X_2(f)=-\int_{-\infty}^{+\infty}g_2(t)\sin(2\pi ft)\mathrm{d}t\end{cases} \tag{25}$$

It can be observed from (25) that $R_1(f)$ and $R_2(f)$ are the even functions with respect to f, while $X_1(f)$ and $X_2(f)$ are the odd functions with respect to f. On this basis, $R_1(f)R_2(f)$ and $X_1(f)X_2(f)$ are the even functions, while $R_1(f)X_2(f)$ and $R_2(f)X_1(f)$ are the odd functions. Therefore, (23) can be further derived as:

$$\begin{aligned}\int_{-\infty}^{+\infty}g_1(t)g_2(t)\mathrm{d}t&=\int_{-\infty}^{+\infty}G_1(f)G_2^*(f)\mathrm{d}f=\\&2\int_0^{+\infty}(R_1(f)R_2(f)+X_1(f)X_2(f))\mathrm{d}f=\\&2\int_0^{+\infty}\mathrm{Re}(G_1(f)G_2^*(f))\mathrm{d}f\end{aligned} \tag{26}$$

By applying (26), (16) can be derived as:

$$\frac{\int_0^{+\infty}\Delta P_{ei}(t)\Delta\omega_i(t)\mathrm{d}t}{\int_0^{+\infty}\Delta\omega_i^2(t)\mathrm{d}t}=\frac{\int_0^{+\infty}\mathrm{Re}(\Delta P_{ei}(f)\Delta\omega_i^*(f))\mathrm{d}f}{\int_0^{+\infty}\mathrm{Re}(\Delta\omega_i(f)\Delta\omega_i^*(f))\mathrm{d}f} \tag{27}$$

Equation (27) implies that EFA is transformed from time domain to frequency domain. Normally, for an oscillation mode with respect to the interested oscillation frequency f_d, (27) can be rewritten as:

$$\frac{\int_0^{+\infty}\Delta P_{ei}^{f_d}(t)\Delta\omega_i^{f_d}(t)\mathrm{d}t}{\int_0^{+\infty}\Delta\omega_i^{f_d}(t)^2\mathrm{d}t}=\frac{\int_0^{+\infty}\mathrm{Re}(\Delta P_{ei}(f_d)\Delta\omega_i^*(f_d))\,\mathrm{d}f}{\int_0^{+\infty}\mathrm{Re}(\Delta\omega_i(f_d)\Delta\omega_i^*(f_d))\,\mathrm{d}f} \tag{28}$$

It should be noted that $\Delta P_{ei}(f_d)$, $\Delta\omega_i(f_d)$ and $\Delta\omega_i^*(f_d)$ are all constant complex numbers at f_d, and hence the integral operator in (28) actually collapses. In fact, the product of $\Delta\omega_i(f_d)$ and $\Delta\omega_i^*(f_d)$ is a real number. Considering the coefficient proposed in (22), (29) can be obtained.

$$K_{de,i}^{f_d}=\mathrm{Re}\left(\frac{\Delta P_{ei}(f_d)\Delta\omega_i^*(f_d)}{\Delta\omega_i(f_d)\Delta\omega_i^*(f_d)}\right)=\mathrm{Re}\left(\frac{\Delta P_{ei}(f_d)}{\Delta\omega_i(f_d)}\right) \tag{29}$$

The following theorem can be summarized by comparing (29) with (7) and (8).

Theorem: for the i^{th} generator, the aggregated damping torque coefficient is essentially equivalent to the frequency-decomposed energy attenuation coefficient with respect to the interested oscillation frequency f_d, i.e.,

$$K_{de,i}^{f_d}=K_{da,i}(f_d) \tag{30}$$

V. Case Studies

The consistency of the proposed coefficients reflecting the damping performance calculated by (8), (22), and (29) is verified by the numerical calculation in both the single-machine

infinite-bus power system and multi-machine power system in this section. The 6th-order model of synchronous generators [26] and the transfer functions of AVR and PSS are given by (A1) and Fig. A1 in the Appendix A.

MATLAB programming is employed to conduct the numerical calculations of $K_{da,i}(f_d)$ and $K_{de,i}^{f_d}$ as follows.

Step 1: assume a set-up disturbance happens at the i^{th} generator in a power system.

Step 2: the time-domain solutions of $P_{ei}(t)$ and $\omega_i(t)$ of the i^{th} generator are obtained by solving the differential equations; then, $\Delta P_{ei}(t)$ and $\Delta\omega_i(t)$ are calculated from $P_{ei}(t)$ and $\omega_i(t)$.

Step 3: the amplitude-frequency characteristic of $\Delta P_{ei}(t)$ is obtained through the Fourier transform, where the frequency of each dominant oscillation mode can be observed; then, an interested oscillation mode at f_d is selected.

Step 4: the modeling is conducted via (3); then, $K_{da,i}(f_d)$ is calculated by substituting A_{21}, $\boldsymbol{A}_{23}$, $\boldsymbol{A}_{31}$, $\boldsymbol{A}_{32}$, $\boldsymbol{A}_{33}$, and f_d into (8).

Step 5: $\Delta P_{ei}(t)$ and $\Delta\omega_i(t)$ are decomposed as $\Delta P_{ei}^{f_d}(t)$ and $\Delta\omega_i^{f_d}(t)$ by applying (18)-(21) with respect to f_d, and then (22) is applied to calculate $K_{de,i}^{f_d}$ in the time domain.

Step 6: (29) is applied to calculate $K_{de,i}^{f_d}$ in the frequency domain.

Finally, the numerical results from (8), (22), and (29) need to be compared to verify the consistency of DTA and EFA.

A. Verification in Single-machine Infinite-bus Power System

The line diagram of a single-machine infinite-bus power system is shown in Fig. 2.

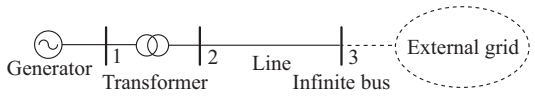

Fig. 2. Line diagram of a single-machine infinite-bus power system.

The parameters of this power system are given in the Appendix B. A step-up disturbance occurs in the mechanical power of the generator at 0.2 s, i.e., P_m=1.1P_{m0}, and lasts for 0.1 s. P_{m0} is the initial mechanical power. There is no installation of PSS. The eigenvalue of the state matrix is computed to be −0.1021+j7.9095.

The simulation results of $\Delta P_e(t)$ and its Fourier transform are shown in Fig. 3. It can be observed that there is only one dominant oscillation mode at around 1.26 Hz.

The simulation results of the angular frequency deviation $\Delta\omega(t)$ and its Fourier transform are given by Fig. 4. It can be observed that there is only one oscillation mode at around 1.26 Hz, which is consistent with the analysis from Fig. 3(b).

In the single-machine infinite-bus power system, the proposed coefficients at 1.26 Hz are calculated by (8), (22), and (29), respectively. The calculation result of the aggregated damping torque coefficient by (8) is 1.6221, and the calculation results of the frequency-decomposed energy attenuation coefficient by (22) and (29) are 1.6054 and 1.6308, respectively, which verifies the consistency.

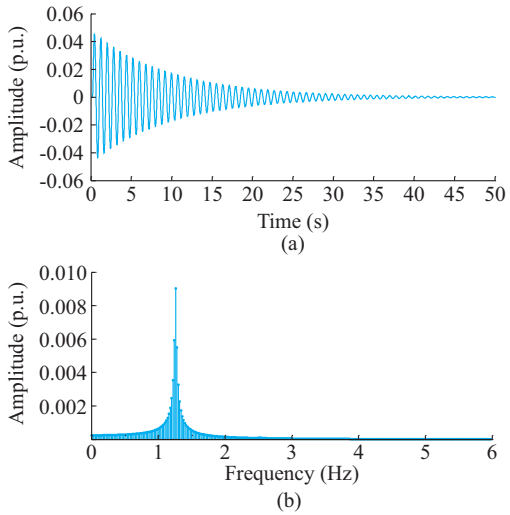

Fig. 3. $\Delta P_e(t)$ and its Fourier transform. (a) $\Delta P_e(t)$ in time domain. (b) Amplitude-frequency characteristic of $\Delta P_e(t)$ in frequency domain.

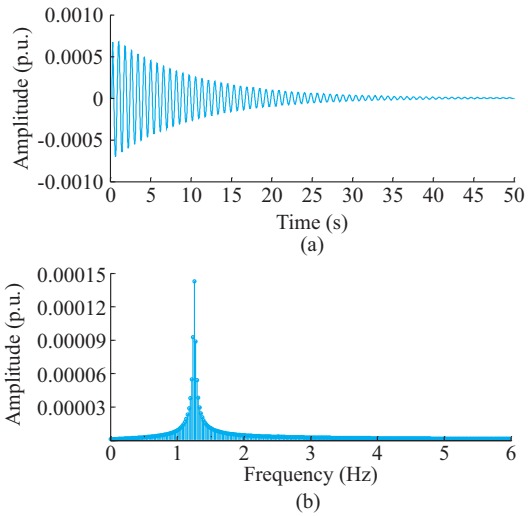

Fig. 4. $\Delta\omega(t)$ and its Fourier transform. (a) $\Delta\omega(t)$ in time domain. (b) Amplitude-frequency characteristic of $\Delta\omega(t)$ in frequency domain.

Generally, the numerical calculation from DTA is considered to be accurate because DTA is a modeling-based method. While the numerical calculation from EFA is regarded as an estimation because EFA is a measurement-based method.

Equation (8) is derived from DTA, (22) is derived from EFA in the time domain and (29) is derived from EFA in the frequency domain. The computing time by (8), (22), and (29) in this single-machine infinite-bus power system is 0.12 s, 0.14 s, and 0.03 s, respectively. Compared with DTA based on (8), the error of EFA based on (22) is −1.03%, while the error of EFA based on (29) is 0.54%. It can be observed that the error of EFA is within an acceptable range.

B. Verification in Multi-machine Power System

A 4-machine 2-area power system is used as an example in this subsection, which is illustrated by Fig. 5. The parameters of the generators, transmission lines, and loads are presented in Appendix C, and the base capacity of this 4-machine 2-area power system is 100 MVA. A step-up distur-

bance occurs in the mechanical power of G_1 at 0.5 s, i.e., P_{m1}= $1.05P_{m1,0}$, and lasts for 0.05 s. $P_{m1,0}$ is the initial mechanical power of G_1.

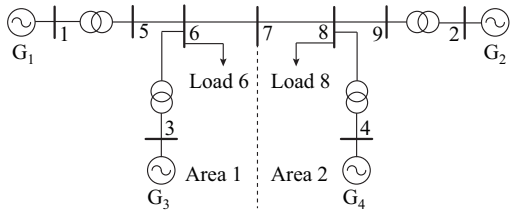

Fig. 5. Line diagram of 4-machine 2-area power system.

The four generators are all equipped with AVR and PSS with the same parameter settings. Three scenarios are designed as follows.

1) Scenario 1: $K_{ai}=60$; $T_{ai}=0.055$ s; $K_{pssi}=8$; $T_{1i}=T_{3i}=5$ s; and $T_{2i}=T_{4i}=3$ s. K_{ai} is the proportional coefficient of AVR of the i^{th} generator. T_{ai} is the time constant of AVR of the i^{th} generator. K_{pssi} is the proportional coefficient of PSS of the i^{th} generator. T_{1i}, T_{2i}, T_{3i}, and T_{4i} are the time constants of PSS of the i^{th} generator.

2) Scenario 2: $K_{ai}=70$; $T_{ai}=0.055$ s; $K_{pssi}=7$; $T_{1i}=T_{3i}=5$ s; and $T_{2i}=T_{4i}=3$ s.

3) Scenario 3: $K_{ai}=80$; $T_{ai}=0.055$ s; $K_{pssi}=6$; $T_{1i}=T_{3i}=5$ s; and $T_{2i}=T_{4i}=3$ s.

As for the neglect of the reactive power in (9), the comparison of the oscillatory energy flow with and without the consideration of the reactive power is conducted at G_1 for Scenario 1. The results are given in Fig. 6. It can be observed that the influence of the reactive power is very small, which can be ignored.

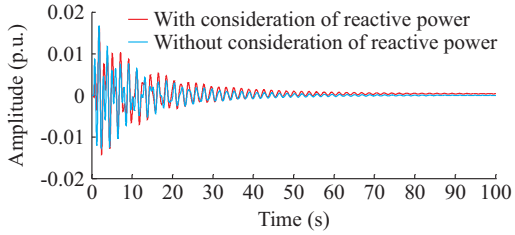

Fig. 6. Oscillatory energy flow with and without consideration of reactive power at G_1 for Scenario 1.

The simulation results of $\Delta P_{e1}(t)$ and its Fourier transform for the three scenarios are shown in Figs. 7-9, respectively. It can be observed that there is an inter-area oscillation mode at 0.53-0.54 Hz, which is the focus of this case study. The eigenvalues of the inter-area oscillation mode for the three scenarios are $-0.0590+\text{j}3.3618$, $-0.0541+\text{j}3.3608$, and $-0.0454+\text{j}3.3580$, respectively. The real part of the eigenvalue indicates the damping [27]. By comparing the real parts of the three eigenvalues, it can be found that the damping performance of Scenario 1 is better.

The calculation results of the aggregated damping torque coefficient by (8) and the frequency-decomposed energy attenuation coefficient by (22) and (29) for the three scenarios are demonstrated by Table I, which shows the consistency.

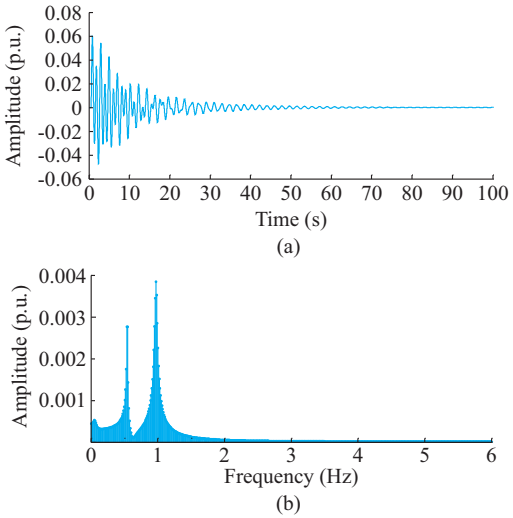

Fig. 7. $\Delta P_{e1}(t)$ and its Fourier transform for Scenario 1. (a) $\Delta P_{e1}(t)$ in time domain. (b) Amplitude-frequency characteristic of $\Delta P_{e1}(t)$ in frequency domain.

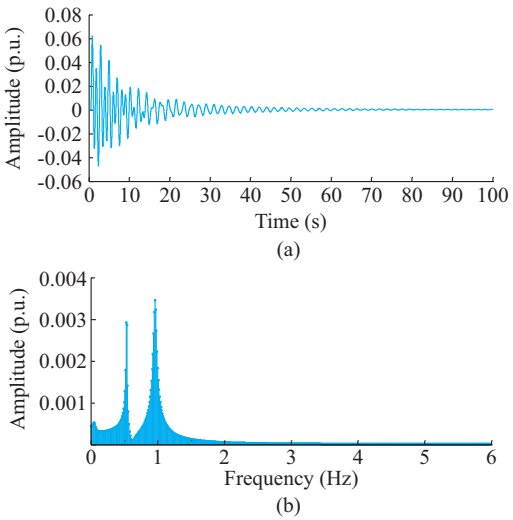

Fig. 8. $\Delta P_{e1}(t)$ and its Fourier transform for Scenario 2. (a) $\Delta P_{e1}(t)$ in time domain. (b) Amplitude-frequency characteristic of $\Delta P_{e1}(t)$ in frequency domain.

The difference between EFA and DTA mainly comes from the following aspects.

1) The fast Fourier transform (FFT) is applied to analyze the amplitude-frequency characteristic of a signal in MATLAB. Since FFT is discrete, the frequency of an oscillation mode may fall between two adjacent spectral lines, which brings a slight error to the presented amplitude.

2) The reactive power is ignored in (9), which leads to a slight error.

3) The integral operation is obtained by accumulating the rectangular areas within the time interval, which causes a slight error. However, the results are generally within the acceptable range.

The damping performance evaluation through different methods is given by Table II, and their evaluation results are consistent. It can be concluded from the case studies that the proposed coefficients can be used as the new indicator for

the damping performance evaluation, which can be obtained from either the time or frequency domain.

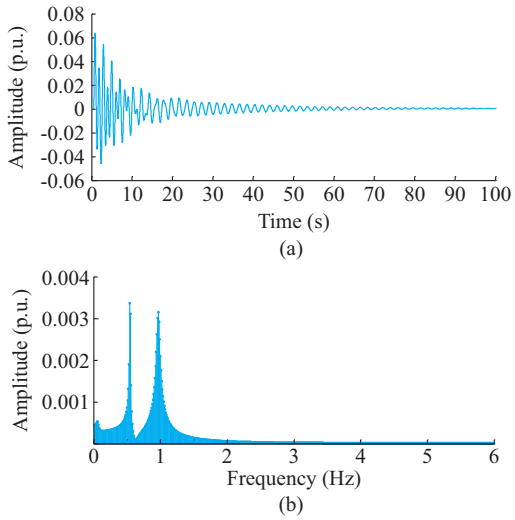

Fig. 9. $\Delta P_{e1}(t)$ and its Fourier transform for Scenario 3. (a) $\Delta P_{e1}(t)$ in time domain. (b) Amplitude-frequency characteristic of $\Delta P_{e1}(t)$ in frequency domain.

TABLE I
CALCULATION RESULTS OF PROPOSED COEFFICIENTS IN 4-MACHINE 2-AREA POWER SYSTEM

Scenario	Calculation result		
	Equation (8)	Equation (22)	Equation (29)
1	44.71	45.34	45.37
2	43.94	44.18	44.21
3	38.93	38.11	38.14

TABLE II
COMPARISON OF DAMPING PERFORMANCE EVALUATION THROUGH DIFFERENT METHODS

Scenario	Eigenvalue-based analysis	DTA	EFA
1	☆☆☆	☆☆☆	☆☆☆
2	☆☆	☆☆	☆☆
3	☆	☆	☆

Note: the number of "☆" indicates the degree of damping performance.

In order to demonstrate the relationship between the real part of eigenvalue (or damping ratio) used by the eigenvalue-based analysis and the proposed coefficients, K_{ai} is randomly adjusted 1000 times between 40 and 80, and K_{pssi} is randomly adjusted 1000 times between 4 and 8. Thus, 1000 simulation scenarios are established to obtain a dense scatter diagram, as shown by the blue scatter points in Figs. 10 and 11, where the fitting result is represented by the red curve. It can be revealed that there is an approximate linear relationship between the proposed coefficients and the real part of the eigenvalue (or damping ratio). In other words, the proposed coefficients provide a new indicator to assess the damping performance of the whole power system, which provides the important reference for the parameter setting of external stabilizers.

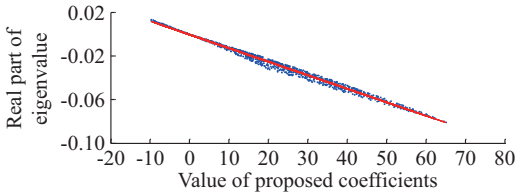

Fig. 10. Relationship between proposed coefficients and real part of eigenvalue.

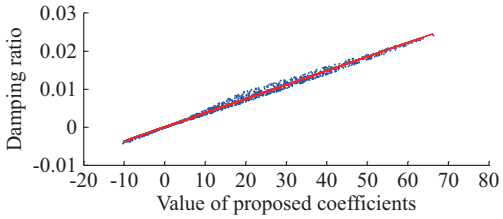

Fig. 11. Relationship between proposed coefficients and damping ratio.

The application of the proposed coefficients to investigate the electromechanical oscillations in power systems is suggested as follows.

In order to evaluate the damping performance based on the aggregated damping torque coefficient, the mathematical models of all power components should be available, and the state-space modeling of the whole power system should be conducted. Then, (8) is applied to calculate the aggregated damping torque coefficient.

The frequency-decomposed energy attenuation coefficient proposed for EFA shows a clear advantage in the large-scale power system with a large number of complex power components. The mathematical models of power components are unnecessary to be known, and the high-dimension modeling can be avoided. In order to evaluate the damping performance based on EFA, the measurements at the terminal of a local generator should be monitored. After that, (22) or (29) can be applied to calculate the frequency-decomposed energy attenuation coefficient.

VI. CONCLUSION

The damping performance evaluation is important to the stable operation of power systems. DTA and EFA are two commonly used methods for the solutions. First, the aggregated damping torque coefficient is defined and derived for DTA to characterize the integration effect of the damping contribution from the whole power system. Then, the preprocessing of measurements at the terminal of a local generator is conducted for EFA, and the frequency-decomposed energy attenuation coefficient is defined to screen and determine the damping contribution with respect to the interested frequency. On this basis, this paper carries out the strict proof on the connection between DTA and EFA in assessing the damping performance of electromechanical oscillations in power systems, which is general for arbitrary synchronous generator models in multi-machine power systems. Specifically, the frequency spectrum analysis of the energy attenuation coefficient reveals that DTA and EFA are essentially equivalent.

After that, case studies are conducted in both the single-machine infinite-bus power system and 4-machine 2-area power system, where the consistency of the aggregated damping torque coefficient and the frequency-decomposed energy attenuation coefficient is numerically verified. Additionally, the relationship between the frequency-decomposed energy attenuation coefficient (or aggregated damping torque coefficient) and the real part of the eigenvalue (or damping ratio) is also disclosed, which further demonstrates the application of the proposed concepts for the damping performance evaluation in power systems.

APPENDIX A

The 6th-order model of synchronous generators is given by (A1). The transfer functions of AVR and PSS of the i^{th} generator are shown in Fig. A1.

$$\begin{cases} \dfrac{\mathrm{d}\delta_i}{\mathrm{d}t} = \omega_0(\omega_i - 1) \\ \dfrac{\mathrm{d}\omega_i}{\mathrm{d}t} = \dfrac{1}{T_{Ji}}[P_{mi} - P_{ei} - D_i(\omega_i - 1)] \\ \dfrac{\mathrm{d}E'_{qi}}{\mathrm{d}t} = \dfrac{1}{T'_{di,0}}(-E_{qi} + E_{fdi}) \\ \dfrac{\mathrm{d}E'_{fdi}}{\mathrm{d}t} = \dfrac{1}{T_{ai}}[-E'_{fdi} + K_{ai}(V_{ti,ref} - V_{ti} + u_{pssi})] \\ \dfrac{\mathrm{d}Y_i}{\mathrm{d}t} = \dfrac{\omega_i - 1 + T_{4i}\dfrac{\mathrm{d}\omega_i}{\mathrm{d}t} - Y_i}{T_{3i}} \\ \dfrac{\mathrm{d}u_{pssi}}{\mathrm{d}t} = \dfrac{K_{pssi}Y_i + K_{pssi}T_{2i}\dfrac{\mathrm{d}Y_i}{\mathrm{d}t} - u_{pssi}}{T_{1i}} \end{cases} \tag{A1}$$

where $T'_{di,0}$ is the time constant of the field winding of the i^{th} generator; V_{ti} is the output voltage of the i^{th} generator; and $V_{ti,ref}$ is the reference output voltage of the i^{th} generator. The meanings of other variables can be found in [26], which are not repeated here.

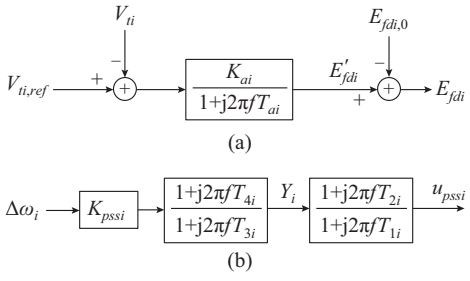

Fig. A1. Transfer functions of AVR and PSS of i^{th} generator. (a) Transfer function of AVR. (b) Transfer function of PSS.

APPENDIX B

The major parameters of the single-machine infinite-bus power system are: $T_J = 8$ s; $D = 0$; $\omega_0 = 314$ rad/s; $T'_{d,0} = 5$ s; $X_d = 0.8$ p.u.; $X_q = 0.4$ p.u.; $X'_d = 0.05$ p.u.; $P_{m0} = 0.6$ p.u.; $X_t = 0.3$ p.u.; $V_1 = V_t = 1.05$ p.u.; $V_2 = 1.0$ p.u.; $V_{t,ref} = 1.05$ p.u.; $K_a = 10$; $T_a = 0.01$ s; $K_{pss} = 0$; $T_2 = T_4 = 0$; and $T_1 = T_3 = 9999$. X_d is the d-axis synchronous reactance; X_q is the q-axis synchronous reactance; X'_d is the d-axis transient reactance; V_1 and V_2 are the voltage at nodes 1 and 2, respectively; and X_t is the reactance of the transmission line and transformer.

APPENDIX C

The major parameters of the 4-machine 2-area power system are: $T_{J1} = T_{J2} = 117$ s; $T_{J3} = T_{J4} = 111.15$ s; $D_1 = D_2 = D_3 = D_4 = 0$; $\omega_0 = 314$ rad/s; $P_{m1,0} = 8.67$ p.u.; $P_{m2,0} = P_{m03,0} = P_{m4,0} = 7.0$ p.u.; $X_{d1} = X_{d2} = X_{d3} = X_{d4} = 0.2$ p.u.; $X_{q1} = X_{q2} = X_{q3} = X_{q4} = 0.1889$ p.u.; $X'_{d1} = X'_{d2} = X'_{d3} = X'_{d4} = 0.0333$ p.u.; $T'_{d1,0} = T'_{d2,0} = T'_{d3,0} = T'_{d4,0} = 8$ s; $V_{t1} = V_{t3} = 1.03$ p.u.; $V_{t2} = V_{t4} = 1.01$ p.u.; $V_{t1,ref} = V_{t3,ref} = 1.03$ p.u.; $V_{t2,ref} = V_{t4,ref} = 1.01$ p.u.; $X_{15} = X_{36} = X_{29} = X_{48} = 0.0167$ p.u.; $X_{56} = X_{89} = 0.025$ p.u.; $X_{67} = X_{78} = 0.055$ p.u.; $P_{load6} = 9.67$ p.u.; $Q_{load6} = 1.00$ p.u.; $P_{load8} = 20.0$ p.u.; $Q_{load8} = 1$ p.u.; $Q_{c6} = -2.0$ p.u.; $Q_{c8} = -3.5$ p.u.. X_{15}, X_{36}, X_{29}, X_{48}, X_{56}, X_{89}, X_{67}, and X_{78} are the reactances of transmission lines and transformers of the 4-machine 2-area power system; P_{load6}, Q_{load6}, P_{load8}, and Q_{load8} are the active power and reactive power at loads 6 and 8 in this 4-machine 2-area power system, respectively; and Q_{c6} and Q_{c8} are the reactive power compensations at the loads 6 and 8, respectively.

REFERENCES

[1] X. Zhang, C. Lu, S. Liu *et al*., "A review on wide-area damping control to restrain inter-area low frequency oscillation for large-scale power systems with increasing renewable generation," *Renewable and Sustainable Energy Reviews*, vol. 57, pp. 45-58, May 2016.

[2] A. Salgotra and S. Pan, "Model based PI power system stabilizer design for damping low frequency oscillations in power systems," *ISA Transactions*, vol. 76, pp. 110-121, May 2018.

[3] D. V. Nair and M. Murty, "Reconfigurable control as actuator fault-tolerant control design for power oscillation damping," *Protection and Control of Modern Power Systems*, vol. 5, no. 1, pp. 1-12, Feb. 2020.

[4] J. Chen, P. Shrestha, S Huang *et al*., "Use of synchronized phasor measurements for dynamic stability monitoring and model validation in ERCOT," in *Proceedings of 2012 IEEE PES General Meeting*, San Diego, USA, Jul. 2012, pp. 1-7.

[5] S. A. N. Sarmadi and V. Venkatasubramanian, "Inter-area resonance in power systems from forced oscillations," *IEEE Transactions on Power Systems*, vol. 31, no. 1, pp. 378-386, Jan. 2016.

[6] J. Ma, P. Zhang, H. Fu *et al*., "Application of phasor measurement unit on locating disturbance source for low-frequency oscillation," *IEEE Transactions on Smart Grid*, vol. 1, no. 3, pp. 340-346, Dec. 2010.

[7] B. Dasu, M. Sivakumar, and R. Srinivasarao, "Interconnected multimachine power system stabilizer design using whale optimization algorithm," *Protection and Control of Modern Power Systems*, vol. 4, no. 1, pp. 1-11, Feb. 2019.

[8] V. L. A. S. V., R. R. Manyala, and S. K. Mangipudi, "Design of a robust PID-PSS for an uncertain power system with simplified stability conditions," *Protection and Control of Modern Power Systems*, vol. 5, no. 3, pp. 202-217, Sept. 2020.

[9] H. Wang and W. Du, *Analysis and Damping Control of Power System Low-frequency Oscillations*. New York: Springer, 2016.

[10] W. Du, H. Wang, and S. Bu, *Small-signal Stability Analysis of Power Systems Integrated with Variable Speed Wind Generators*. Cham: Springer, 2018.

[11] S. Bu, X. Zhang, J. Zhu *et al*., "Comparison analysis on damping mechanisms of power systems with induction generator based wind power generation," *International Journal of Electrical Power and Energy Systems*, vol. 97, pp. 250-261, Apr. 2018.

[12] S. Xia, S. Bu, X. Zhang *et al*., "Model reduction strategy of doubly-fed induction generator-based wind farms for power system small-signal rotor angle stability analysis," *Applied Energy*, vol. 222, pp. 608-620, Jul. 2018.

[13] S. Bu, W. Du, and H. Wang, "Model validation of DFIGs for power system oscillation stability analysis," *IET Renewable Power Genera-*

tion, vol. 11, no. 6, pp. 858-866, May 2017.
[14] F. J. Swift and H. Wang, "The connection between modal analysis and electric torque analysis in studying the oscillation stability of multi-machine power systems," *International Journal of Electrical Power and Energy Systems*, vol. 19, no. 5, pp. 321-330, Jun. 1997.
[15] W. Du, J. Bi, C. Lv *et al*., "Damping torque analysis of power systems with DFIGs for wind power generation," *IET Renewable Power Generation*, vol. 11, no. 1, pp. 10-19, Jan. 2017.
[16] W. Du, X. Chen, and H. Wang, "Power system electromechanical oscillation modes as affected by dynamic interactions from grid-connected PMSGs for wind power generation," *IEEE Transactions on Sustainable Energy*, vol. 8, no. 3, pp. 1301-1312, Jul. 2017.
[17] Y. Ge, W. Du, T. Littler *et al*., "Damping torque analysis of AVR in large-scale multi-machine power systems," in *Proceedings of 2nd IET Renewable Power Generation Conference*, Beijing, China, Sept. 2013, pp. 1-4.
[18] L. G. Meegahapola, S. Bu, D. P. Wadduwage *et al*., "Review on oscillatory stability in power grids with renewable energy sources: monitoring, analysis, and control using synchrophasor technology," *IEEE Transactions on Industrial Electronics*, vol. 68, no. 1, pp. 519-531, Jan. 2021.
[19] J. Zhao, Y. Zhang, P. Zhang *et al*., "Development of a WAMS based test platform for power system real time transient stability detection and control," *Protection and Control of Modern Power Systems*, vol. 1, no. 1, pp. 1-11, Jun. 2016.
[20] Y. Yu, Y. Min, L. Chen *et al*., "Disturbance source location of forced power oscillation using energy functions," *Automation of Electric Power Systems*, vol. 34, no. 5, pp. 1-6, Mar. 2010.
[21] S. Maslennikov, B. Wang, and E. Litvinov, "Dissipating energy flow method for locating the source of sustained oscillations," *International Journal of Electrical Power and Energy Systems*, vol. 88, pp. 55-62, Jun. 2017.
[22] R. Xie and D. J. Trudnowski, "Tracking the damping contribution of a power system component under ambient conditions," *IEEE Transactions on Power Systems*, vol. 33, no. 1, pp. 1116-1117, Jan. 2018.
[23] L. Chen, Y. Min, and W. Hu, "Low frequency oscillation analysis and oscillation source location based on oscillation energy–Part one: mathematical foundation and energy flow computation," *Automation of Electric Power Systems*, vol. 36, no. 3, pp. 22-27, Feb. 2012.
[24] L. Chen, Y. Chen, Y. Min *et al*., "Low frequency oscillation analysis and oscillation source location based on oscillation energy–Part two: method for oscillation source location and case studies," *Automation of Electric Power Systems*, vol. 36, no. 4, pp. 1-5, Feb. 2012.
[25] L. Chen, Y. Min, Y. Chen *et al*., "Relationship between oscillation energy analysis and eigenvalue analysis and assessment of generator damping," *Automation of Electric Power Systems*, vol. 37, no. 19, pp. 33-40, Oct. 2013.
[26] X. Wang, Y. Song, and M. Irving, *Modern Power Systems Analysis*. New York: Springer, 2008.
[27] L. Chen, F. Xu, Y. Min *et al*., "Transient energy dissipation of resistances and its effect on power system damping," *International Journal of Electrical Power and Energy Systems*, vol. 91, pp. 201-208, Oct. 2017.

Yong Hu received the B.Eng. degree in electrical engineering and automation from Agricultural University of Hebei, Baoding, China, in 2014, and the M.Eng. degree in electrical engineering from Beijing Jiaotong University, Beijing, China, in 2017. He is currently pursuing the Ph.D. degree in the Department of Electrical Engineering, The Hong Kong Polytechnic University, Hong Kong, China. His research interests include oscillatory stability analysis of power systems with renewable energy generations, optimal strategies for improving power system stability, and optimal planning as well as operation of smart grids with renewable energy generations.

Siqi Bu received the Ph.D. degree from the Electric Power and Energy Research Cluster, The Queen's University of Belfast, Belfast, UK, in 2012, where he continued his postdoctoral research work before entering industry. Then he was with National Grid, Wokingham, UK, as an experienced UK National Transmission System Planner and Operator. He is currently an Associate Professor with The Hong Kong Polytechnic University, Hong Kong, China, and also a Chartered Engineer with UK Royal Engineering Council, London, UK. He is a Senior Member of IEEE. His research interests include power system stability analysis and operation control with the integration of wind power generation, plug-in electric vehicle, HVDC, flexible AC transmission system, energy storage system and virtual synchronous generator.

Xin Zhang is a Senior Lecturer (Associate Professor) in Energy Systems at Cranfield University, Cranfield, UK. He used to work at National Grid, Wokingham, UK, for power system real-time operation. He is a Chartered Engineer and a Senior Member of IEEE. His research interests include power system planning and operation with renewable energy, and grid interaction with land-air transport electrification.

Chi Yung Chung received the B.Eng. (with First Class Honors) and the Ph.D. degrees in electrical engineering from The Hong Kong Polytechnic University, Hong Kong, China, in 1995 and 1999, respectively. He is currently a Professor, the NSERC/SaskPower (Senior) Industrial Research Chair in smart grid technologies, and the SaskPower Chair in power systems engineering in the Department of Electrical and Computer Engineering, University of Saskatchewan, Saskatoon, Canada. He is also an IEEE PES Distinguished Lecturer and a member of IEEE PES Fellows Evaluation Committee. His research interests include smart grid technologies, renewable energy, power system stability/control, planning and operation, computational intelligence applications, power markets and electric vehicle charging.

Hui Cai received the Ph.D. degree from The Queen's University of Belfast, Belfast, UK, the master's degree from RWTH Aachen University, Aachen, Germany. He is currently working in State Grid Jiangsu Economic Research Institute, Nanjing, China. His research interests include transmission system planning, applications of FACTS devices in real systems, dynamic stability analysis with FACTS and HVDC integration.